

GENERAL ARTICLE

LRRK2 interacts with the vacuolar-type H⁺-ATPase pump a1 subunit to regulate lysosomal function

Rebecca Wallings[†], Natalie Connor-Robson and Richard Wade-Martins^{*}

Oxford Parkinson's Disease Centre, Department of Physiology, Anatomy and Genetics, University of Oxford, South Parks Road, Oxford OX1 3QX, UK

^{*}To whom correspondence should be addressed at: Oxford Parkinson's Disease Centre, Department of Physiology, Anatomy and Genetics, University of Oxford, South Parks Road, Oxford OX1 3QX, UK. Tel: +44 (0)1865 282837; Email: richard.wade-martins@dpag.ox.ac.uk

Abstract

Lysosomal dysfunction lies at the centre of the cellular mechanisms underlying Parkinson's disease although the precise underlying mechanisms remain unknown. We investigated the role of leucine-rich repeat kinase 2 (LRRK2) on lysosome biology and the autophagy pathway in primary neurons expressing the human LRRK2-G2019S or LRRK2-R1441C mutant or the human wild-type (hWT-LRRK2) genomic locus. The expression of LRRK2-G2019S or hWT-LRRK2 inhibited autophagosome production, whereas LRRK2-R1441C induced a decrease in autophagosome/lysosome fusion and increased lysosomal pH. *In vivo* data from the cortex and substantia nigra pars compacta of aged LRRK2 transgenic animals revealed alterations in autophagosome puncta number reflecting those phenotypes seen *in vitro*. Using the two selective and potent LRRK2 kinase inhibitors, MLI-2 and PF-06447475, we demonstrated that the LRRK2-R1441C-mediated decrease in autolysosome maturation is not dependent on LRRK2 kinase activity. We showed that hWT-LRRK2 and LRRK2-G2019S bind to the a1 subunit of vATPase, which is abolished by the LRRK2-R1441C mutation, leading to a decrease in a1 protein and cellular mislocalization. Modulation of lysosomal zinc increased vATPase a1 protein levels and rescued the LRRK2-R1441C-mediated cellular phenotypes. Our work defines a novel interaction between the LRRK2 protein and the vATPase a1 subunit and demonstrates a mode of action by which drugs may rescue lysosomal dysfunction. These results demonstrate the importance of LRRK2 in lysosomal biology, as well as the critical role of the lysosome in PD.

Introduction

Parkinson's disease (PD) is a common progressive neurodegenerative disease, affecting ~1–2% of the population over the age of 65 years (1). Mutations in the gene encoding leucine-rich repeat kinase 2 (LRRK2) are the most frequent cause of familial PD (2), and cases have an indistinguishable clinico-pathological phenotype from sporadic PD. LRRK2 polymorphisms are also associated with increased risk of sporadic PD (3), suggesting that LRRK2 may provide understanding of the molecular mecha-

nisms of both sporadic and genetic diseases. Pathogenic mutations are found in the enzymatic domains of the LRRK2 protein. The LRRK2-G2019S mutation in the kinase domain leads to an increase in kinase activity (4), a potential pathogenic mechanism of LRRK2 that is further supported by the protective effects of LRRK2 kinase inactivation (5,6). Located in the GTPase domain of LRRK2, Arg¹⁴⁴¹ is the second most common site of pathogenic LRRK2 substitutions (LRRK2-R1441C/G), leading to decreased GTP hydrolysis (7,8) and motor deficits and defects in dopaminergic neurotransmission in rodent models (9,10,11,12).

[†]Rebecca Wallings, <http://orcid.org/0000-0003-0947-4459>

Received: February 20, 2019. Revised: February 20, 2019. Accepted: April 15, 2019

© The Author(s) 2019. Published by Oxford University Press.

This is an Open Access article distributed under the terms of the Creative Commons Attribution License (<http://creativecommons.org/licenses/by/4.0/>), which permits unrestricted reuse, distribution, and reproduction in any medium, provided the original work is properly cited.

Lysosomes are cytoplasmic membrane-enclosed organelles containing hydrolytic enzymes that degrade macromolecules and cell components. Many factors regulate lysosomal function and subsequent protein degradation such as lysosomal pH (13), calcium release (14) and membrane trafficking (15). Lysosomal function decreases with age, with a rise in lysosomal pH (16). Lysosomal dysfunction has been shown to lead to the accumulation of α -synuclein (17), which may play a role in the build-up of Lewy bodies, the pathological hallmark of PD. Neurons are especially vulnerable to deficiencies in autophagy substrate clearance. Without the aid of cell division, which decreases the burden of intracellular waste in mitotic cells, neurons are largely dependent on autophagy to prevent the accumulation of cellular protein and damaged organelles. The crucial role of lysosomes in PD is reinforced by the observation that genes involved in lysosomal function, such as *VPS35* (18), *ATP6VOA1* (19), *ATP13A2* (20), *GBA* (21) and *LIMP2* (22), have repeatedly been associated with the disease.

Autophagy is a multifaceted pathway, from substrate recognition and autophagosome formation to autophagosome-lysosome fusion and lysosomal protein degradation. LRRK2 localizes to autophagic compartments and has been implicated in mechanisms underlying the regulations of these steps (23,24). Increased autophagic flux with LRRK2 kinase inhibition has been reported (25), suggesting an inhibitory effect of LRRK2 on autophagy induction. Local calcium release from lysosomes has been shown to be required for lysosome fusion (14). Alterations in the autophagy pathway caused by LRRK2 have been reported to be rescued by an NAADP receptor antagonist (26), suggesting a mechanistic role of LRRK2 in lysosomal calcium homeostasis. Lysosomal degradation is highly dependent on lysosomal pH and substantial shifts in pH can severely disrupt both degradative enzyme activity and fusion of autophagosomes and lysosomes (25). LRRK2 has been implicated in lysosomal pH regulation in different model systems (26,27). It is likely, therefore, that LRRK2 does not simply regulate autophagy induction as previously assumed, but is instead involved throughout the pathway, with a critical role at the lysosome.

To advance our understanding of the impact of LRRK2 mutations on the autophagy/lysosomal pathway, primary neuronal cultures were prepared from LRRK2 bacterial artificial chromosome (BAC) transgenic rats expressing either the human LRRK2-G2019S, or LRRK2-R1441C, or the wild-type (WT) form (hWT-LRRK2) of the entire human LRRK2 genomic locus (9). Neurons expressing human LRRK2-G2019S or hWT-LRRK2 exhibit a decrease in the rate of autophagosome formation, whereas neurons expressing human LRRK2-R1441C, but not LRRK2-G2019S and hWT-LRRK2, demonstrate a deficit in autophagosome-lysosome fusion, leading to decreased lysosome-mediated degradation. These phenotypes were also observed *in vivo* in aged animals, with an increase in LC3 levels in both cortical neurons and dopamine neurons of the substantia nigra pars compacta of LRRK2-R1441C animals. *In vitro*, we found that the decrease in autolysosome maturation in LRRK2-R1441C neurons was not dependent on LRRK2 kinase activity, whereas the phenotypes observed in LRRK2-G2019S and hWT-LRRK2 cortical neurons were kinase-dependent. LRRK2-R1441C cultures also exhibited decreased lysosomal acidity and alterations in lysosomal calcium dynamics. We found that hWT-LRRK2 interacts with the α 1 subunit of the v-type H^+ ATPase proton pump (vATPase α 1), which is responsible for regulating lysosomal pH. Furthermore, the LRRK2-R1441C mutation abolished this interaction, dysregulating vATPase α 1 protein expression and cellular localization. Finally, clioquinol,

was capable of rescuing LRRK2-R1441C deficits through modulation of lysosomal zinc content. The increase in zinc content in lysosomes increased v-ATPase α 1 subunit protein levels, corrected lysosomal pH, increased localized lysosomal calcium release and rescued the autophagosome/lysosome fusion deficit in LRRK2-R1441C neurons. These findings provide key insights both into the mechanisms by which LRRK2 impacts autophagy in PD and the modes of action of potentially-therapeutic drugs.

Results

LRRK2-R1441C neurons exhibit alterations in basal autophagy

Primary cortical neuronal cultures from LRRK2 BAC transgenic P1 rat pups were generated and characterized for expression of the human LRRK2 transgene (using the transgenic N-terminal YPet protein tag) (9) and endogenous *Lrrk2* protein expression. hWT-LRRK2 and LRRK2-R1441C neurons express similar levels of each LRRK2 transgene, whereas LRRK2-G2019S cultures express a 2–3-fold higher level of transgene relative to both hWT-LRRK2 and LRRK2-R1441C (Fig. 1A). Co-immunofluorescence staining for transgene protein and the neuronal marker MAP2 confirmed transgene presence in neurons (Fig. 1B). hWT-LRRK2 and LRRK2-R1441C transgene expression is 2–3-fold higher than endogenous *Lrrk2* levels, and LRRK2-G2019S transgene expression is 5–6-fold higher (Supplementary Material, Fig. S1a), confirming previous published data from these animals (9).

Expression of autophagy-related proteins was measured to assess basal autophagy levels in cortical neuronal cultures. LRRK2-R1441C neuronal cultures exhibited a significant increase in LC3-II (Fig. 1C), although no significant differences in LAMP1 or p62 expression were observed (Supplementary Material, Fig. S1b,c). Primary cortical cultures contained a mixed population of cells, comprising 30–40% neurons (Supplementary Material, Fig. S1d,e). Co-immunofluorescence staining for the autophagy proteins LC3 and LAMP1 to quantify autophagosomes and autolysosomes demonstrated LRRK2-R1441C neurons showed a significant increase in autophagosome number and a significant decrease in autolysosome number (Fig. 1D and E; Supplementary Material, Fig. S1f). No significant changes in lysosome size were observed between genotypes (Supplementary Material, Fig. S1g).

Assessing LC3 expression changes in cortical and midbrain tissue of aged animals

To understand whether the LRRK2-R1441C-dependent autophagy phenotype was present *in vivo* in brain tissue from aged animals, 22-month-old rat cortical sections were stained for LC3 and puncta quantified in MAP2+ cells (Supplementary Material, Fig. S2a). Cortical neurons from aged LRRK2-R1441C rats showed a significant increase in LC3 puncta number (Supplementary Material, Fig. S2b), with no change in puncta size (Supplementary Material, Fig. S2c). Midbrain sections containing the substantia nigra pars compacta were stained for LC3 and puncta quantified in tyrosine hydroxylase-positive (TH+) dopamine neurons (Supplementary Material, Fig. S2d). Interestingly, nigral dopamine neurons in the midbrain of both LRRK2-R1441C and LRRK2-G2019S animals demonstrated a significant increase in LC3 puncta (Supplementary Material, Fig. S2e), with no difference in LC3 puncta size (Supplementary

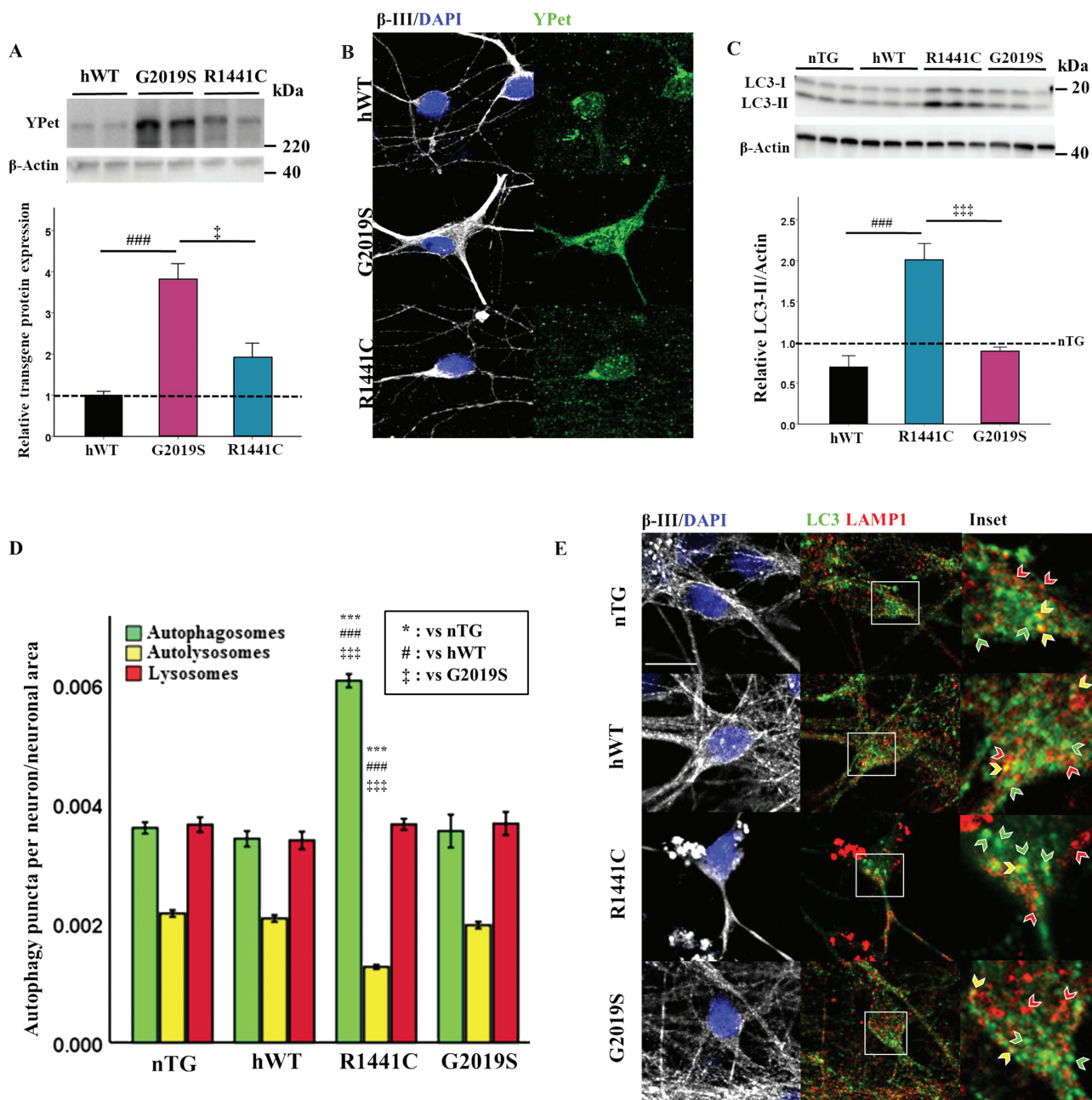


Figure 1. LRRK2-R1441C neurons exhibit alterations in basal autophagy. (A) Primary cortical neuronal cultures from P1 pups were generated and characterized. Western blots for YPet expression were quantified to assess transgene protein level and normalized to hWT levels. (B) Cultures at DIV 14 were stained for MAP2 and YPet to assess transgene expression in neurons. (C) Western blots for LC3-II were quantified and normalized to nTG littermate controls (dotted line = nTG normalized average; bars = mean \pm SEM; N = 3; *P < 0.05, ***P < 0.001; one-way ANOVA, Tukey HSD post hoc). (D, E) DIV 14 primary cortical cultures were fixed and stained for β -III, LC3 and LAMP1, confocal images acquired and autophagy puncta number per neuron quantified and normalized to neuronal area. Bars represent mean \pm SEM. (N = 3; ***P < 0.001; Kruskal-Wallis non-parametric ANOVA, Bonferroni post hoc). *, versus nTG; #, versus hWT; †, versus G2019S. Scale bar = 5 μ m. Arrow heads: red, lysosome; yellow, autolysosome; green, autophagosome.

Material, Fig. S2f). Therefore, although the effects of the LRRK2-R1441C mutation are present in different neuronal cell types, the effects of LRRK2-G2019S on the autophagy pathway might be cell-type dependent.

LRRK2-R1441C neurons exhibit decreased autolysosome maturation

Steady state LC3-II protein levels and autophagy puncta counts can be difficult to interpret in terms of overall flux through

the autophagy pathway as both induction of autophagy, or the inhibition of autophagosome clearance, could explain the increases observed. However, a decrease in autolysosome maturation indicates an inhibition of autophagosome clearance. LC3-II protein expression and autophagy puncta fold changes were assessed in the presence of modulators of the autophagy pathway to discriminate between these two possibilities. In the presence of chloroquine or bafilomycin a1, autophagic flux, as assessed by LC3-II expression changes by western blotting, was significantly decreased in LRRK2-R1441C primary

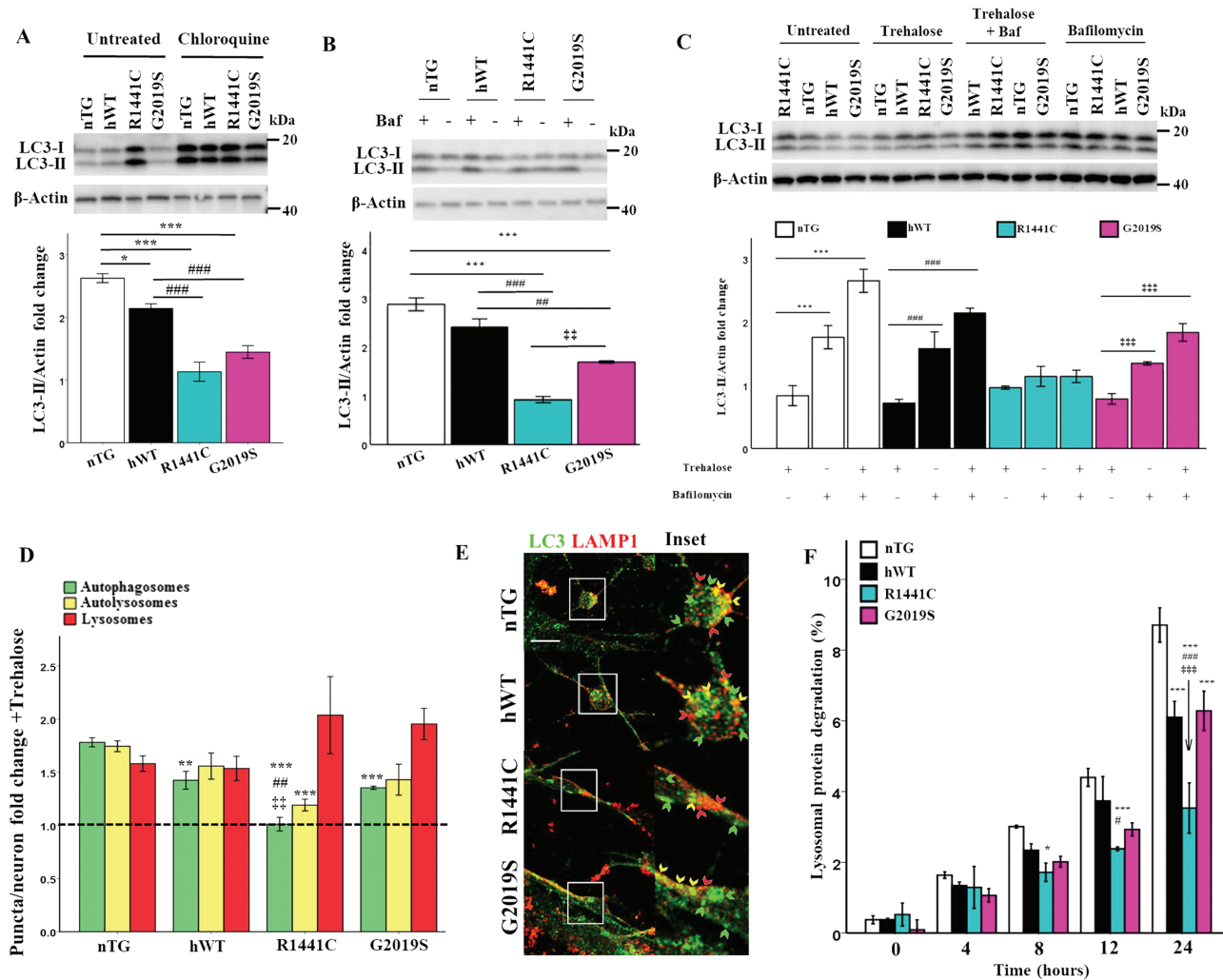


Figure 2. LRRK2-R1441C neurons have decreased autolysosome maturation, which cannot be rescued by lysosome biogenesis. (A, B) Western blots for LC3-II were quantified to assess LC3-II fold change from basal in response to treatment with 20 μM chloroquine for 8 h or 10 nM bafilomycin a1 for 2 h. (C) DIV 14 primary cortical neuronal cultures were treated with 500 μM trehalose for 24 h and/or 10 nM bafilomycin a1 for 2 h and western blots for LC3-II were quantified to measure changes in autophagic flux. Bars, mean \pm SEM (N=3; *P < 0.05; **P < 0.005; ***P < 0.001; two-way ANOVA, Bonferroni post hoc). (D, E) DIV 14 primary cortical neuronal cultures were treated with 500 μM trehalose for 24 h, fixed and stained for LC3 and LAMP1 and puncta per neuron normalized to neuronal size quantified to measure fold change. Dotted line represents basal puncta number/neuron. Bars, mean \pm SEM (N=3; ***P < 0.005; ****P < 0.001; Kruskal-Wallis non-parametric ANOVA, Bonferroni post hoc). Scale bar = 5 μm . Arrow heads: red, lysosome; yellow, autolysosome; green, autophagosome. (F) DIV 14 primary cortical neuronal cultures were incubated with radiolabelled valine for 48 h and CPM was measured over 24 h in untreated cultures or in the presence of chloroquine to calculate lysosomal protein degradation. Bars, mean \pm SEM (N=3; *P < 0.05; **P < 0.005; ***P < 0.001; two-way ANOVA, Bonferroni post hoc). *, versus nTG; #, versus hWT; +, versus G2019S.

cortical cultures (Fig. 2A and B). In order to assess if this altered autophagic flux was present in neurons in these cortical cultures, co-immunofluorescence for LC3 and LAMP1 was performed. The autolysosome count for LRRK2-R1441C neurons did not decrease with chloroquine as observed in the other three genotypes (Supplementary Material, Fig. S3a, b). Taken together, these data suggest a block in autophagosome clearance and a deficit in autolysosome maturation in LRRK2-R1441C neurons, as opposed to an increase in autophagy induction. Interestingly, both hWT-LRRK2 and LRRK2-G2019S neurons demonstrate a significant decrease in autophagic flux as assessed by western blotting, which reflected a decrease in autophagosome fold-change relative to nTG with chloroquine treatment, with no differences seen in autolysosome fold-change as measured by co-immunofluorescence, indicating inhibited autophagosome biogenesis.

To assess whether the accumulation of autophagosomes in LRRK2-R1441C neurons could be rescued by increasing lysosome number, neuronal cultures were treated with 500 μM trehalose, a compound known to induce lysosomal biogenesis (28). Increased LAMP1 expression was observed with a 24-h trehalose treatment in all genotypes, indicating an increase in lysosomes (Supplementary Material, Fig. S3c). Both autophagic flux, as assessed by changes in LC3-II expression in the presence of trehalose and bafilomycin a1, and autolysosomal fold-change from basal levels remained significantly decreased in LRRK2-R1441C neurons compared to nTG (Fig. 2C–E), suggesting an inherent autophagosome-lysosome fusion deficiency in these neurons. Furthermore, there was a significant decrease in autophagosome fold-change from basal levels in all three hLRRK2 genotypes compared to non-transgenic neurons, suggesting an inhibitory effect of hLRRK2 expression on autophagosome production.

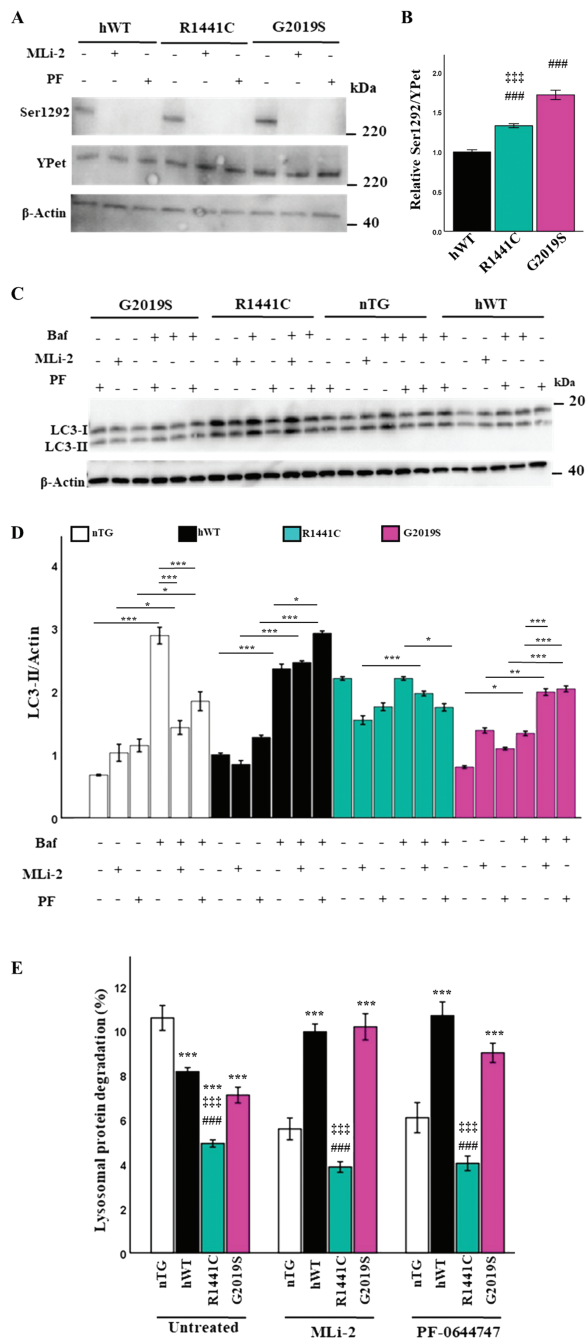


Figure 3. LRRK2-R1441C autophagy phenotype is not dependent on LRRK2 kinase activity (A, B) Primary cortical neuronal cultures at DIV 14 were treated with the LRRK2 kinase inhibitors (50 nM MLI-2 for 1 h or 50 nM PF-06447475 for 1 h) and assessed for expression of total YPet-tagged LRRK2 and phosphorylated LRRK2 at Ser1292 by western blot. (B) Proportion of Ser1292 phosphorylated YPet-tagged LRRK2 at basal levels was quantified by western blot. Bars, mean \pm SEM (N=3; ***P < 0.001; Kruskal-Wallis non-parametric ANOVA, Bonferroni post hoc). *, versus nTG; #, versus hWT; †, versus G2019S. (C, D) DIV 14 primary neuronal cultures were treated with 50 nM MLI-2, 50 nM PF-06447475 for 1 h or 10 nM Bafilomycin a1 for 2 h or in combination and LC3-II expression quantified to assess changes in autophagic flux. Bars, mean \pm SEM (N=3; *P < 0.05; **P < 0.005; ***P < 0.001; two-way ANOVA, Bonferroni post hoc). (E) DIV 14 primary cortical neuronal cultures were incubated with radiolabelled valine for 48 h and CPM was measured over 24 h in untreated cultures or in the presence of MLI-2 or PF-06447475 to calculate lysosomal protein degradation. Bars, mean \pm SEM (N=3; ***P < 0.001; three-way ANOVA, Bonferroni post hoc). *, versus nTG; #, versus hWT; †, versus G2019S.

LRRK2-R1441C neuronal cultures exhibit decreases in lysosomal protein degradation

To assess whether decreases in autolysosome maturation were coupled with changes in lysosomal protein degradation, a pulse-chase assay using C^{14} -radiolabelled valine was carried out based on the protocol developed by Gronostajski and Pardee (29). The data demonstrate that in LRRK2-R1441C neuronal cultures lysosomal protein degradation was significantly decreased (Fig. 2F). Furthermore, hWT-LRRK2 and LRRK2-G2019S cultures had decreased lysosomal protein degradation compared to nTG controls at the final 24-h time point but were still significantly greater compared to LRRK2-R1441C cultures. These changes in protein degradation reflect the changes seen in autophagy puncta counts and autophagic flux already described and confirm that the presence of hWT-LRRK2 or LRRK2-G2019S inhibits the production of autophagosomes, whereas LRRK2-R1441C is capable of decreasing autolysosome maturation.

The LRRK2-R1441C autophagy phenotype is not dependent on LRRK2 kinase activity

The overexpression of the LRRK2 kinase domain as well as inhibition of LRRK2 kinase activity induces alterations of the autophagy-lysosomal pathway (26,30). Primary cortical neuronal cultures were prepared and treated with 50 nM of the selective and potent LRRK2 inhibitors MLI-2 and PF-06447475 for 2 h, and LRRK2 phosphorylation levels were measured to confirm that kinase activity had been decreased (Fig. 3A). At basal conditions, an increase in phosphorylated LRRK2 at Ser1292 was observed in LRRK2-G2019S and LRRK2-R1441C cultures relative to hWT-LRRK2 (Fig. 3B). LC3-II protein levels were assessed by western blot to observe potential downstream effects of LRRK2 kinase inhibition on autophagy. hWT-LRRK2 and LRRK2-G2019S cultures both demonstrated increased autophagic flux in response to both MLI-2 and PF-06447475 treatment, while no significant changes were seen in LRRK2-R1441C cultures (Fig. 3C and D). Interestingly, the LRRK2 kinase inhibitors had the opposite effect on endogenous Lrrk2 in nTG cultures, decreasing autophagic flux. In order to confirm that observed alterations in LC3-II levels were dependent on LRRK2 kinase inhibition as opposed to off-target effects, *Lrrk2*^{-/-} primary cortical neuronal cultures were treated with MLI-2. No changes in LC3-II levels were observed in *Lrrk2*^{-/-} cultures with MLI-2 treatment relative to WT litter mate controls (Supplementary Material, Fig. S3e, f).

We next performed pulse-chase assays to quantify protein degradation in response to LRRK2 kinase inhibition. Lysosomal protein degradation was significantly increased in the presence of the LRRK2 kinase inhibitors in both hWT-LRRK2 and LRRK2-G2019S cultures (Fig. 3E), correlating with the increase in LC3-II protein levels as measured by flux assays. LRRK2-R1441C cultures, however, showed no significant changes in protein degradation levels with kinase inhibition. Finally, a significant decrease in lysosomal protein degradation was also observed in nTG primary neuronal cultures with MLI-2 and PF-06447475 treatment correlated with the decrease in LC3-II protein expression.

LRRK2-R1441C neurons have impaired lysosome pH

Both lysosomal degradation and autophagosome/lysosome fusion are highly dependent on lysosomal pH. As defects in autolysosome maturation were evident in LRRK2-R1441C

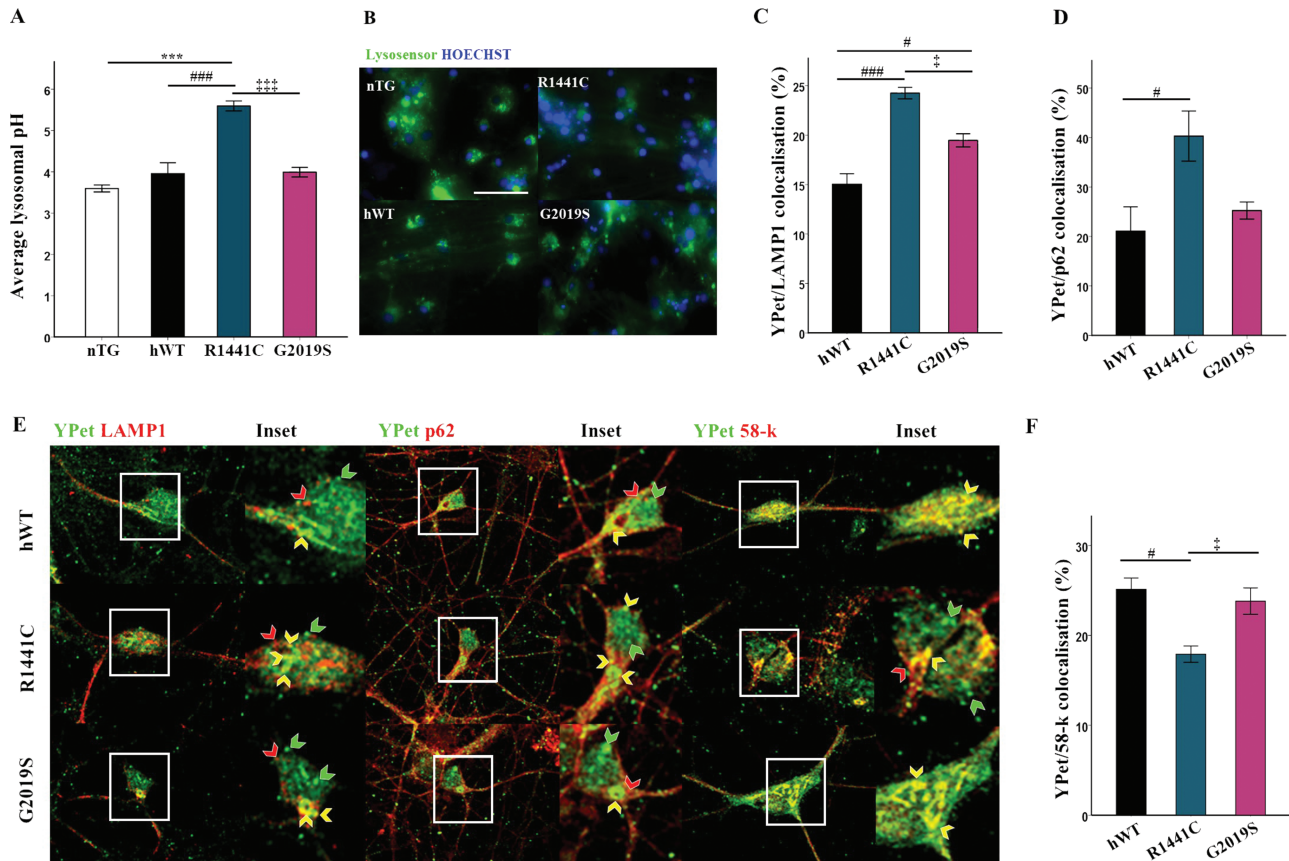


Figure 4. LRRK2-R1441C neuronal cultures exhibit increased lysosomal pH and co-localization with autophagic proteins. (A, B) Using the pH sensitive dye lysosensor lysosomal pH was quantified in primary cortical neuronal cultures from P1 pups at DIV 14. Bars, mean \pm SEM (N=3; ***P < 0.001; Kruskal-Wallis non-parametric ANOVA, Bonferroni post hoc). Scale bar=200 μ m. (C, D, E) DIV 14 primary cortical neuronal cultures were fixed and stained for YPet and LAMP1/p62/58-k and colocalization quantified. Bars, mean \pm SEM (N=3; *P < 0.05; ***P < 0.001; one-way ANOVA, Bonferroni post hoc). (F) Representative confocal images of YPet and LAMP1/p62/58-k staining. Scale bar = 10 μ m. Red arrow, LAMP1/p62/58-k only; green arrow, YPet only; yellow arrow, YPet co-localization with LAMP1/p62/58-k.

neurons, we asked if altered lysosomal pH could account for the compromised vesicle fusion. Lysosomal pH was measured using the pH sensitive dye, LysoSensorTM Green DND-189, which exhibits increased fluorescence in acidic organelles, using a pH/fluorescence standard curve in cells incubated in pH-calibrated solutions (Supplementary Material, Fig. S3a). Measurement of average lysosomal pH across genotypes demonstrated that lysosomal pH was significantly increased in LRRK2-R1441C expressing cultures, with an average lysosomal pH of 5.5 (Fig. 4A and B).

The LRRK2-R1441C mutations alters LRRK2 cellular localization

It has been reported that mutant and WT LRRK2 co-localize with markers of the autophagy pathway (23). Co-immunofluorescence staining in LRRK2-R1441C primary neurons demonstrated an increase in LRRK2-R1441C co-localization with the autophagy markers P62 and LAMP1 compared to both hWT-LRRK2 and LRRK2-G2019S cultures (Fig. 4C-E; Supplementary Material, Fig. S4b). Interestingly, all transgenic neurons exhibited skein-like hLRRK2-positive structures revealed using the YPet tag as previously reported in cell lines harbouring the LRRK2-R1441C BAC constructs (23). Further co-immunofluorescence demonstrated that such skein-like structures show discrete co-localization to the trans-Golgi marker, 58 k (Fig. 4E; Supplementary Material, Fig. S4b). Furthermore, LRRK2-R1441C neurons exhibited

decreased co-localization of hLRRK2 to the trans-Golgi marker compared to hWT-LRRK2 and LRRK2-G2019S neurons (Fig. 4F). The decreased co-localization of LRRK2-R1441C to the trans-Golgi, and its increased co-localization to autophagic puncta, is a potential mechanism by which mutations alter hLRRK2 normal function.

Increased autophagic flux and lysosomal protein degradation are observed in *Lrrk2*^{-/-} neurons

Primary neuronal cultures were prepared from *Lrrk2* knock-out (*Lrrk2*^{-/-}) rats to compare the loss-of-function phenotype with mutant autophagy phenotypes likely caused by a gain of function. *Lrrk2* expression in primary cortical cultures was first assessed to confirm knockout at the protein level (Supplementary Material, Fig. S5a). A significant increase in LC3-II protein levels was observed in *Lrrk2*^{-/-} primary neurons compared to WT littermates (Supplementary Material, Fig. S5b) with no changes in LAMP1 or p62 protein expression observed (Supplementary Material, Fig. S5c, d). *Lrrk2*^{-/-} primary cortical neuronal cultures and WT litter mate controls were treated with 20 μ m chloroquine and LC3-II expression levels by western blotting were quantified in order to assess autophagic flux (Supplementary Material, Fig. S5e). A trend of increased autophagic flux was observed in *Lrrk2*^{-/-} cultures, which did not reach significance (Supplementary Material, Fig. S5f). However, using the more sensitive pulse-chase assay demonstrated that knock-out of the

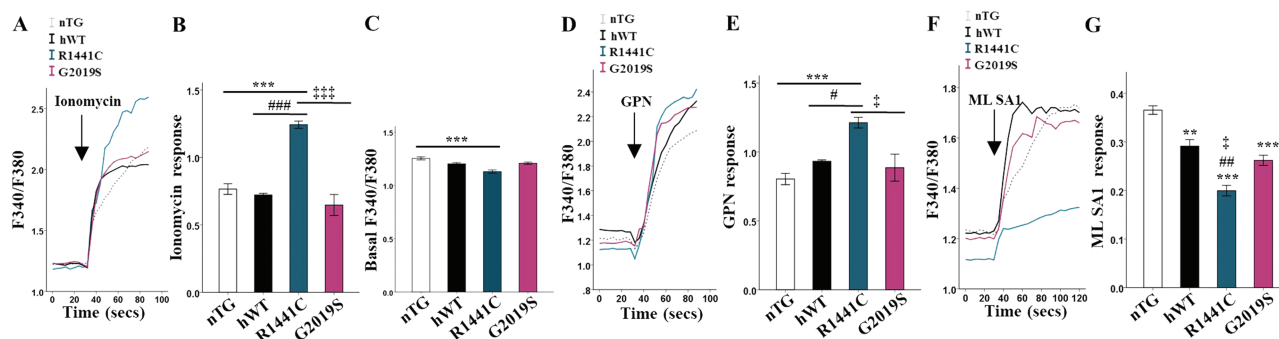


Figure 5. LRRK2-R1441C neurons have impaired lysosome calcium dynamics. (A, B) DIV 14 primary cortical neuronal cultures were incubated with the Fura2AM and fluorescence ratio quantified at basal and after the injection of ionomycin and delta quantified. (C) Baseline Fura2-AM was quantified across all lines to assess cytosolic Ca²⁺ content. (D, E) GPN was used in order to quantify lysosomal Ca²⁺ content. (F, G) ML SA1 was used in order to quantify Ca²⁺ release from TRPML1 channels. Bars, mean \pm SEM (N=3; *P < 0.05; **P < 0.005; ***P < 0.001; Kruskal-Wallis non-parametric ANOVA, Bonferroni post hoc). *, versus nTG; #, versus hWT; †, versus G2019S.

Lrrk2 protein was associated with an increase in lysosomal protein degradation (Supplementary Material, Fig. S5g). Overall, these data are consistent with WT Lrrk2 having a physiological function of reducing autophagic activity.

LRRK2-R1441C neurons have impaired lysosome calcium dynamics

Local calcium release from lysosomes is required for late endosome-lysosome fusion (14). We therefore measured calcium signalling from different intracellular stores in LRRK2-G2019S and LRRK2-R1441C mutant primary neuronal cultures using the ratiometric calcium sensitive dye, Fura2-AM. We first showed a significantly increased whole-cell calcium content in LRRK2-R1441C cultures assayed by the response to ionomycin (Fig. 5A and B). It was also observed that LRRK2-R1441C expression induced a significantly decreased fluorescence ratio at basal levels prior to compound administration (Fig. 5C). Together this suggests an increase in intracellular calcium stores and a decrease in cytosolic calcium levels. We then administered compounds to assess the calcium content of specific organelles. The lysosome-disrupting compound, GPN, (Fig. 5D and E) led to an increased response in LRRK2-R1441C cultures. The increase in whole-cell calcium content in response to ionomycin was therefore likely caused by alterations in lysosomal calcium as no significant differences between genotypes in response to FCCP or CPA were observed (Supplementary Material, Fig. S6a, b, c, d) indicating no changes in mitochondria or ER calcium content, respectively.

The transient receptor potential cation channel, mucolipin subfamily, member 1 (TRPML1), is a cation channel located on lysosomal membranes and is one of the channels responsible for the local release of calcium. We used ML SA1, a compound capable of inducing TRPML1-mediated calcium release, to investigate release from lysosomes. We observed a significantly decreased lysosomal calcium release in response to ML SA1 in the LRRK2-R1441C cultures (Fig. 5F and G). Such decreased local calcium release may explain the decrease in fusion efficiency seen between the autophagosomes and lysosomes.

LRRK2 interacts with vATPase a1 that is abolished by the LRRK2-R1441C mutation

The a1 subunit of the vATPase proton pump is enriched in neurons in the transmembrane V₀ subcomplex of the vATPase,

which is trafficked to and from the Golgi to the lysosome where it is able to form the full vATPase complex with the V₁ subcomplex and regulate lysosomal pH levels. Protein level quantification revealed the a1 subunit to be downregulated in LRRK2-R1441C cultures and was also upregulated in LRRK2-G2019S cultures (Fig. 6A). Co-immunoprecipitation with YPet in hLRRK2-transgenic cell lysates was performed in order to assess binding to ATP6V0A1. hWT-LRRK2 and LRRK2-G2019S protein was observed to bind to this subunit; however, this interaction is abolished in the LRRK2-R1441C protein (Fig. 6B). nTG lysates were subject to co-immunoprecipitation with YPet in order to assess non-specific binding (Supplementary Material, Fig. S6e).

To confirm the observations in the co-immunoprecipitations, vATPase a1-YPet-tagged LRRK2 co-localization was assessed by co-immunofluorescence. A significant decrease in vATPase a1 co-localization to LRRK2-R1441C, relative to hWT-LRRK2, was observed (Fig. 6C and D; Supplementary Material, Fig. S6f). The vATPase a1 subunit is localized to the lysosomal membrane and is trafficked from the Golgi to its cellular target. The correct binding of vATPase a1 to interaction partners mediates this trafficking. vATPase a1 co-localization to both the Golgi and lysosomes was therefore assessed. A significant decrease in vATPase a1-LAMP1 co-localization was observed in LRRK2-R1441C neurons relative to both hWT-LRRK2 and LRRK2-G2019S. Furthermore, a significant increase was observed in LRRK2-G2019S neurons, relative to hWT-LRRK2 (Fig. 6E and F; Supplementary Material, Fig. S6f). A significant decrease in vATPase a1/58-k co-localization was also observed in both LRRK2-R1441C and LRRK2-G2019S neurons relative to hWT-LRRK2 (Fig. 6G and H; Supplementary Material, Fig. S6f). vATPase a1 protein expression was assessed by western blotting in an enriched lysosome cell fraction to confirm this phenotype with a biochemical assay. Lysosome fractions were enriched for LAMP1 expression, while the trans-Golgi marker, 58-k, was reduced (Fig. 6I). vATPase a1 expression was significantly reduced in lysosome fractions from LRRK2-R1441C primary cortical neuronal cultures relative to hWT and LRRK2-G2019S cultures. Furthermore, LRRK2-G2019S primary cortical neuronal cultures demonstrated increased vATPase a1 expression in purified lysosome samples relative to hWT-LRRK2 and LRRK2-R1441C (Fig. 6J). Overall, the loss of interaction between LRRK2-R1441C and vATPase a1 is associated with the mislocalization of vATPase a1. Furthermore, the increase in vATPase a1 protein expression in LRRK2-G2019S primary cortical neuronal cultures is associated with increased vATPase a1 localization to the lysosome in these neurons.

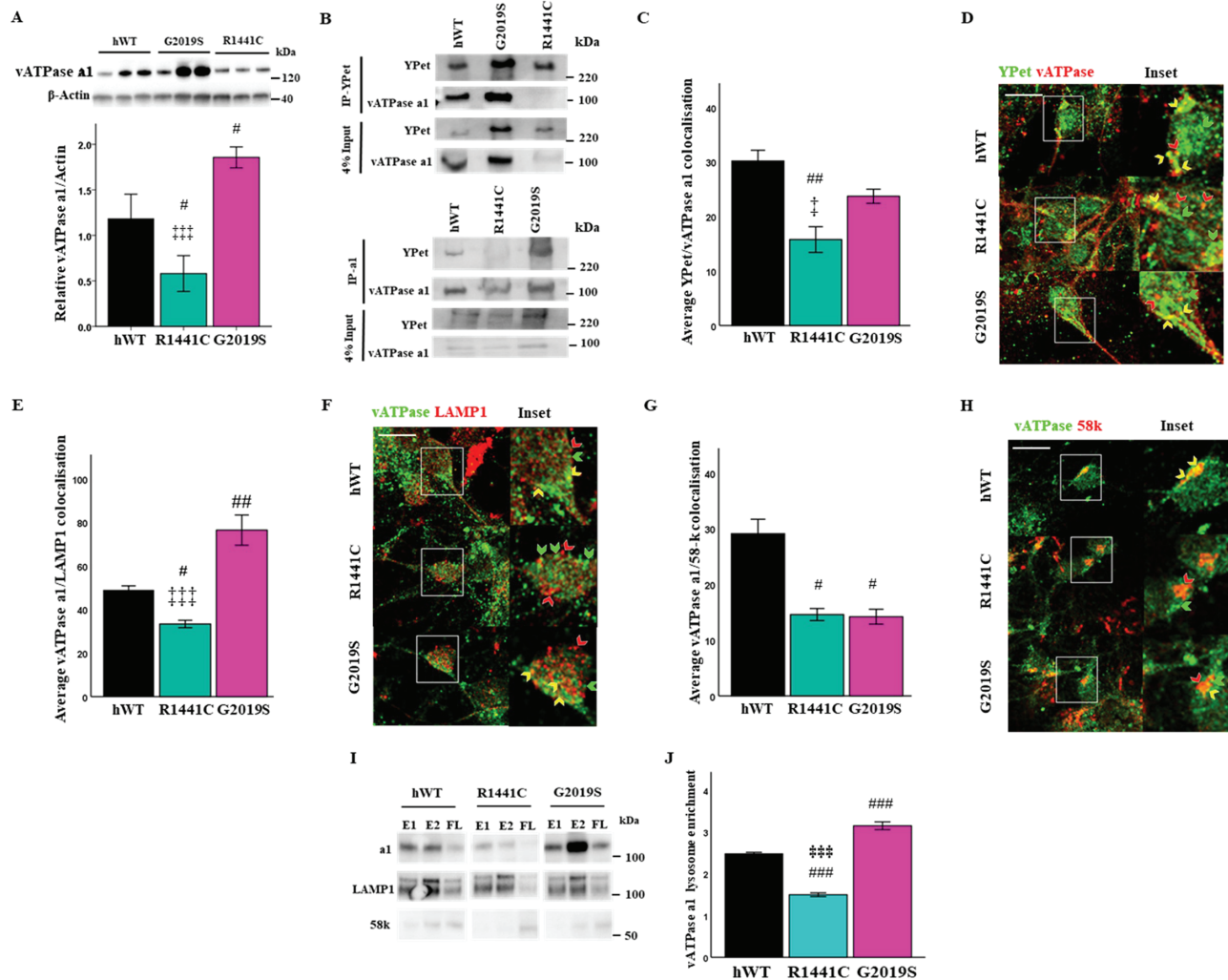


Figure 6. LRRK2 directly interacts with vATPase a1, which is abolished by the LRRK2-R1441C mutation. (A) Western blots for vATPase a1 were quantified to assess basal protein levels. Bars, mean \pm SEM (N=3; *P < 0.05; ***P < 0.001; Kruskal–Wallis non-parametric ANOVA, Bonferroni post hoc). (B) YPet and vATPase a1 were immunoprecipitated from LRRK2 transgenic primary cortical neuronal cultures at DIV 14 and vATPase a1/YPet protein expression observed. (C, D) DIV 14 primary cortical neuronal cultures were fixed and stained for YPet, vATPase a1 and β -III tubulin and co-localization percentage quantified. Co-localization between vATPase a1 and LAMP1 (E, F) or the Golgi marker 58-k (G, H) was quantified in DIV 14 cortical cultures. Scale bar = 10 μ m. Arrows: red, red channel only; green, green channel only; yellow, co-localization of red and green channels. (I, J) Lysates from primary cortical neuronal cultures at DIV 14 were ultracentrifuged and lysosome-enriched fractions collected. vATPase a1, LAMP1 and 58-k protein expression were assessed in lysosome enriched fractions by western blot and quantified relative to flow-through (average densitometry value of E1 and E2 relative to FL; E1 = enriched fraction 1, E2 = enriched fraction 2, FL = flow-through). Bars, mean \pm SEM (N=3; *P < 0.05; **P < 0.01; ***P < 0.001; one-way ANOVA, Bonferroni post hoc). #, versus hWT; †, versus G2019S.

Clioquinol rescues the LRRK2-R1441C cellular phenotypes

It was recently reported that clioquinol, a zinc/copper ionophore, induces a cellular transcriptomic response anti-correlated to transcriptomic perturbations observed when comparing human LRRK2-G2019S with control induced pluripotent stem cell-derived dopamine neurons (31). To better understand the effect of clioquinol on the key LRRK2 mutant cellular phenotypes we observe in primary neurons, autophagic flux, autophagy puncta counts, lysosomal pH levels and protein-degradation assays were performed in the presence of the compound. Treatment of primary cortical neuronal cultures with clioquinol increased LC3-II flux in LRRK2-R1441C cultures (Fig. 7A) and significantly increased autolysosome counts in LRRK2-R1441C neurons (Fig. 7B and C; Supplementary Material, Fig. S7a, b). The LRRK2-R1441C lysosomal pH was also significantly re-acidified

from basal levels in response to clioquinol (Fig. 7D and E). The presence of clioquinol increased lysosomal calcium release in LRRK2-R1441C primary cultures in response to ML SA1, indicating a correction of TRPML1 channel function (Fig. 7F; Supplementary Material, Fig. S7e), while total lysosomal calcium content increased (Supplementary Material, Fig. S7d, e). Furthermore, clioquinol was capable of increasing lysosomal protein degradation in LRRK2-R1441C cortical cultures as indicated by the pulse-chase assay (Fig. 7G).

Clioquinol modulates lysosomal zinc levels and upregulates vATPase a1 protein

Previous reports have suggested that clioquinol may increase lysosomal zinc levels, which then act to modulate pH (32). We therefore used the zinc-sensitive dye, Furo-Zin3, to determine

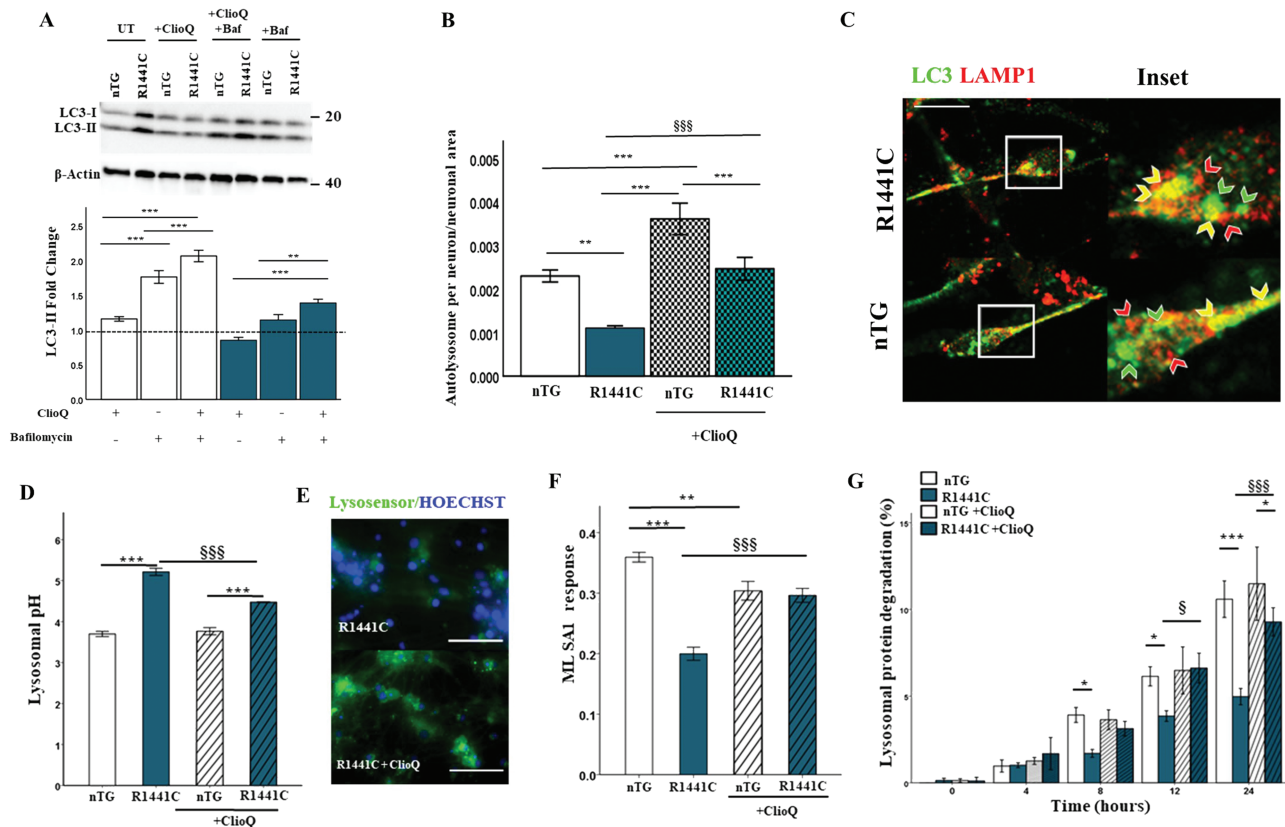


Figure 7. Clioquinol rescues autophagy related deficits in LRRK2-R1441C neuronal cultures. (A) DIV 14 primary cortical neuronal cultures were treated with 1 μ M clioquinol for 48 h and/or 10 nM bafilomycin a1 for 2 h and LC3-II protein expression assessed to evaluate changes in autophagic flux. (B, C) DIV 14 primary cortical neuronal cultures were fixed and stained for LC3 and LAMP1 in β -III tubulin+ cells and autolysosomes/neuron normalized to neuronal size was quantified to assess changes in response to 1 μ M clioquinol for 48 h. Scale bar = 5 μ m. (D, E) Lysosomal pH was quantified in response to 1 μ M clioquinol. Scale bar = 200 μ m. (F) Primary cortical neuronal cultures were incubated in Fura2-AM and lysosomal calcium response to ML SA1 was measured either in the presence of or without 1 μ M clioquinol pre-treatment. Bars, mean \pm SEM. (N = 3; *P < 0.05; **P < 0.01; ***P < 0.001; two-way ANOVA, Bonferroni post hoc). (G) DIV 14 primary cortical neuronal cultures were incubated with radiolabelled valine for 48 h, and CPM was measured over 24 h in untreated cultures or in the presence of 1 μ M clioquinol to calculate lysosomal protein degradation. Bars, mean \pm SEM (N = 3; *P < 0.05; ***P < 0.001; three-way ANOVA, Bonferroni post hoc). *, versus nTG; §, versus R1441C.

the effect of clioquinol on lysosomal zinc levels in LRRK2-R1441C primary cortical neuronal cultures. We observed that clioquinol treatment significantly increased Furo-Zin3-positive lysosomes in LRRK2-R1441C, but not nTG cultures (Fig. 8A; Supplementary Material, Fig. S7f). Treatment of cortical cultures with the zinc chelator N,N,N',N'-tetrakis(2-pyridylmethyl)ethane-1,2-diamine (TPEN) decreased Furo-Zin3 fluorescence (Supplementary Material, Fig. S7g), confirming specificity of this dye. We next investigated if lysosomal zinc levels may functionally upregulate, or increase protein expression of, vATPase a1. Clioquinol treatment significantly upregulated protein expression of the a1 subunit of vATPase in LRRK2-R1441C primary cortical neuronal cultures (Fig. 8B), without changing lysosomal number as assayed by lysotracker (Supplementary Material, Fig. S7h).

In order to experimentally determine whether the effects of clioquinol of LRRK2-R1441C phenotype were zinc dependent, the clioquinol rescue assays previously described were repeated in the presence of the TPEN. In the presence of TPEN, clioquinol was no longer able to significantly increase vATPase a1 protein levels, nor decrease lysosomal pH from basal levels in LRRK2-R1441C cultures (Fig. 8B and C, Supplementary Material, Fig. S7i). Similarly, alterations in calcium release from TRPML1 channels were no longer increased with clioquinol treatment when co-treated with TPEN (Fig. 8D and E). Using the pulse-chase assay, in the presence of TPEN, lysosomal protein degradation decreased

back to levels comparable to basal (Fig. 8F). Together these data provide strong evidence for the essential role of zinc in clioquinol rescue in LRRK2-R1441C neuronal cultures.

Discussion

Our work has demonstrated differential effects on the autophagy/lysosomal pathway by the LRRK2-R1441C and hWT-LRRK2 and LRRK2-G2019S variants in primary neuronal cultures. We have shown that the LRRK2-R1441C mutation prevents the normal binding of LRRK2 protein to the a1 subunit of vATPase, which leads to increased lysosomal pH and dysregulated lysosomal calcium dynamics through decreased a1 subunit protein levels and its mislocalization, inhibiting the maturation of autolysosomes. The LRRK2-R1441C phenotypes were shown to be independent of LRRK2 kinase activity. Furthermore, the LRRK2-R1441C autophagic deficits were not limited to primary cortical neurons, as increased LC3 expression was observed in both cortical neurons and dopamine neurons of the nigra in aged LRRK2-R1441C animals. These observations place the LRRK2-R1441C mutation as acting at the lysosome, specifically at the point of autophagosome-lysosome fusion. By modulating lysosomal zinc content and increasing vATPase subunit protein levels, clioquinol is capable of rescuing the

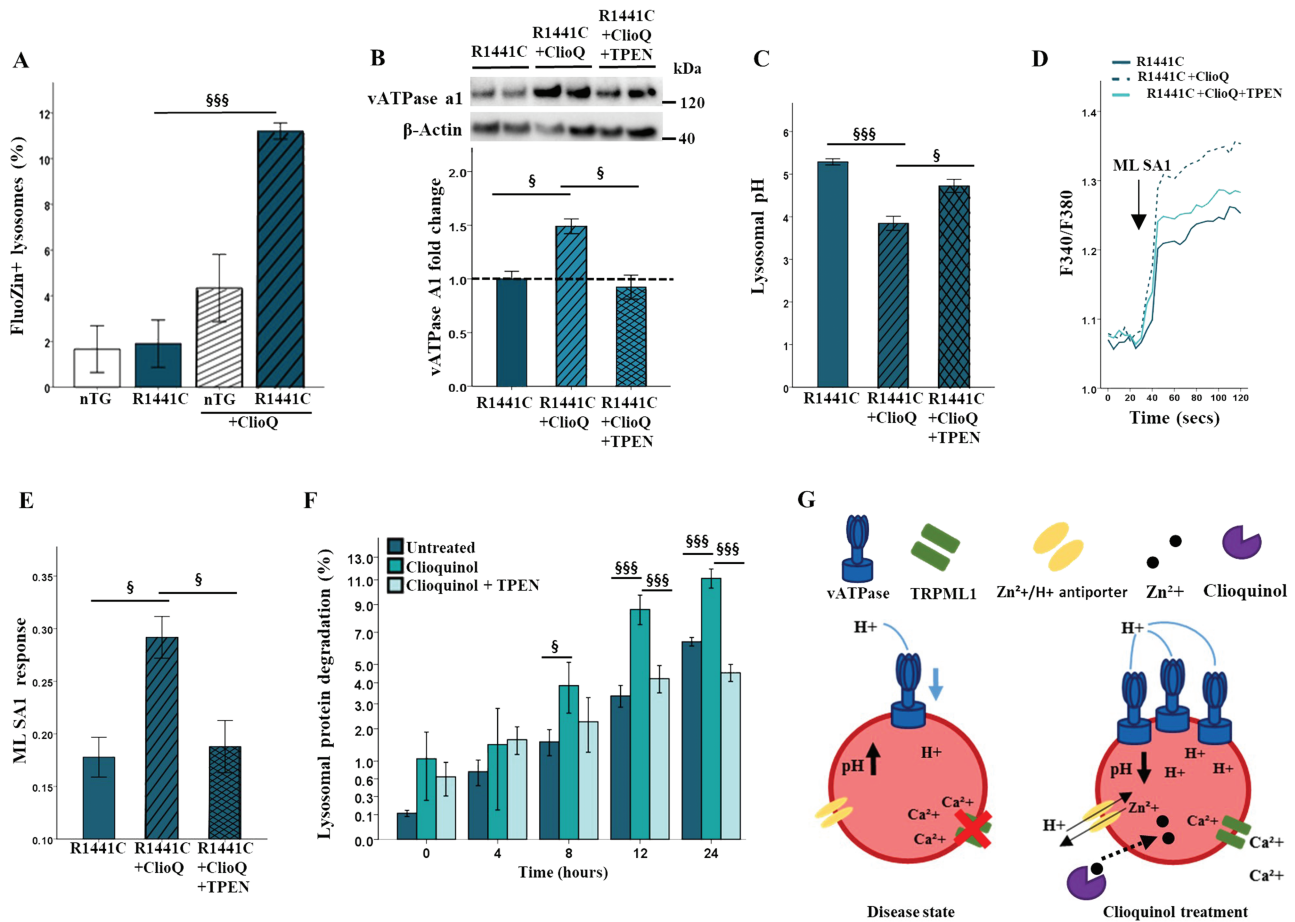


Figure 8. Clioquinol modulates lysosomal zinc levels and increase expression of vATPase a1. (A, B) Using the zinc-sensitive dye FluoZin-3 and the lysosome dye lysotracker, the percentage of FluoZin3+ lysosomes was quantified in the presence or absence of 1 μ M clioquinol after 48 h. Bars, mean \pm SEM (N=3; ***P < 0.001; two-way ANOVA, Bonferroni post hoc). (B) Western blots for vATPase a1 in LRRK2-R1441C primary neuronal cultures in the presence or absence of 1 μ M clioquinol for 48 h and 500 nM TPEN for 6 h were quantified. (C) Using the pH sensitive dye lysosensor, lysosomal pH was quantified in LRRK2-R1441C primary cortical neuronal cultures treated with 1 μ M clioquinol. (D, E) ML SA1 was used to quantify calcium release from TRPML1 channels after 1 μ M clioquinol treatment. Bars, mean \pm SEM. (N=3; *P < 0.05, ***P < 0.001; one-way ANOVA, Tukey HSD post hoc). (F) DIV 14 LRRK2-R1441C primary cortical neuronal cultures were incubated with radiolabelled valine for 48 h and CPM was measured over 24 h in untreated cultures or in the presence of 500 nM TPEN and/or 1 μ M clioquinol to calculate lysosomal protein degradation. Bars, mean \pm SEM (N=3; *P < 0.05; **P < 0.005; ***P < 0.001; two-way ANOVA, Bonferroni posthoc, §, versus R1441C). (G) Schematic diagram of disease phenotype and effect of clioquinol treatment on the lysosome.

observed autolysosome maturation deficit by correcting both pH and calcium release from TRPML1 channels, providing a novel mechanism to correct lysosomal dysfunction in PD.

The kinase-dependent decrease in autophagic flux described here with hWT-LRRK2 and LRRK2-G1029S expression, combined with the increases observed in *Lrrk2*^{-/-} neurons, suggests that the expression of either hWT-LRRK2 or LRRK2-G2019S inhibits the production of autophagosomes, a phenotype that has previously been reported (25,33,34). It has recently been reported that LRRK2 is able to inhibit the autophagy pathway by its interaction with Beclin1-containing class II PI3-kinase (25). Furthermore, this Beclin1 complex has been reported to be found to co-localize with trans-Golgi makers (35). The co-localization of hWT-LRRK2 and LRRK2-G2019S to the trans-Golgi could therefore underlie the inhibitory role of LRRK2 on the autophagy pathway demonstrated here. Many validated and potential LRRK2 targets are involved in pathways converging and diverging on the TGN. For example, Rab8 and Rab10 have been validated as true LRRK2 targets (36) and both of these GTPases have been implicated in biosynthetic trafficking from the TGN to the ER and plasma membrane (37,38).

Autophagy phenotypes were also replicated *in vivo*, with LRRK2-R1441C neurons in aged cortical and nigral tissue exhibiting increased LC3-positive puncta, demonstrating that alterations in autophagic activity induced by the LRRK2-R1441C mutation are not specific to cultured cortical neurons. Interestingly, although no significant changes in LC3 expression were observed in the cortex of LRRK2-G2019S animals, increased LC3 expression was observed in dopamine neurons of the substantia nigra pars compacta of these animals, which may contribute to the selective vulnerability of these dopamine neurons due to increased metabolic pressure (39). It has also been previously suggested that, although LRRK2 is ubiquitously expressed, LRRK2 is expressed at different levels in different brain regions (40). These differences, as well as the identification of specific functions of LRRK2 within specific systems such as the immune system (40,41), supports the hypothesis that LRRK2 could play different roles within different cell types and tissue.

LRRK2-R1441C neurons exhibited increased lysosomal pH, a critical phenotype for the decreased autolysosome maturation described. Substantial shifts in pH, such as those induced by drugs like chloroquine, severely disrupt degradative enzyme

activity and also block fusion of autophagosomes and lysosomes (13). Elevations in lysosomal pH have previously been reported in cellular models in Alzheimer's disease (42,43), and lysosome dysfunction is increasingly placed at the centre of neurodegenerative disease pathways. Increased lysosomal pH would not only decrease lysosomal fusion capacity and lysosomal enzyme activity, but has also been reported to have much more far-reaching consequences. Altered lysosomal degradation induces axonal transport impairment (45) and increases oxidized lipids and reactive oxygen species (45), leading to lysosomal membrane permeabilization resulting in apoptosis and necrosis (46).

The $\alpha 1$ subunit of the vATPase proton pump was found to be mislocalized in the presence of LRRK2-R1441C, presumably due to the loss in LRRK2-vATPase $\alpha 1$ interaction observed. Interestingly, in a recent meta-analysis of genome-wide association studies ATP6V0A1, encoding the vATPase $\alpha 1$ subunit was identified as a novel PD risk loci (19). This highlights not only the crucial role of the lysosome in PD but also the potential interplay between PD genetic risk factors. This same subunit has been shown to become destabilized in Presenilin-1 knock-out (PS1KO) cells, a model of Alzheimer's disease, leading to elevated lysosomal pH (47). Furthermore, the blocking or knock-down of this sub-unit was capable of replicating the reported lysosomal phenotypes in PS1KO cells. The N-terminus of this subunit is essential for vATPase function because it serves to tether V1 to the membrane and must withstand the torque generated by V1 during motor movement (48). In addition, this region contains the information necessary for correct targeting of vATPases to cellular destinations (49). It is intriguing, therefore, that it is this subunit that LRRK2 interacts with and is downregulated in LRRK2-R1441C cultures. It has previously been demonstrated that modulation of vATPase $\alpha 1$ binding partners can negatively affect its function and lead to autolysosome maturation deficits similar to what has been described here (50). It has recently been shown that the membrane-anchored $\alpha 1$ subunit of the vATPase undergoes S-palmitoylation on Cys-25 and that expression is significantly decreased in palmitoyl-protein thioesterase 1 (Ppt1) deficient mice (51). Furthermore, dynamic palmitoylation (palmitoylation-depalmitoylation) facilitates the degradation of proteins that undergo palmitoylation (52). Therefore, alterations in vATPase $\alpha 1$ palmitoylation in LRRK2-R1441C cultures may underlie the decrease in vATPase $\alpha 1$ expression levels.

We have shown that LRRK2 kinase inhibition is able to ameliorate the inhibitory effect of hWT-LRRK2 and LRRK2-G2019S on autophagosome biogenesis, consistent with previous findings (25). However, kinase inhibitors had no effect on LRRK2-R1441C phenotypes, suggesting that kinase activity may not be critical to the lysosomal phenotypes. It may be that the differential effects of the LRRK2-G2019S and LRRK2-R1441C mutations on lysosomal dysfunction may reside in differences in GTPase activity in these two mutations, and that the GTPase domain may be critical to the role of LRRK2 at the lysosome. Although the LRRK2-G2019S mutation consistently increases kinase activity (53,54,55,56), reports on the effect of other LRRK2 mutations residing in the kinase domain and in the GTPase domain on LRRK2-kinase activity have been inconsistent (4,7,53,55). Furthermore, mutants with hyperactive GTPase (R1298L) or inactive GTPase (R1398L/T1343 V) cannot mimic the G2019S phenotypes (57). While mutations in the GTPase domain have been reported to decrease GTP hydrolysis (58,59,60), the G2019S mutation has no discernible effects on GTPase activity (61). Taken together, it seems that mutations residing in different enzymatic domains exert different effects on the enzymatic activity of LRRK2, which impact cellular function in different ways. Understanding how

LRRK2 GTPase activity contributes to cellular phenotypes is challenging and may require genetic or pharmacological manipulation of the GTPase domain.

Our work supports a mechanistic role for LRRK2 in calcium signalling in agreement with the effects on lysosomal calcium homeostasis previously reported (26). We demonstrate here that LRRK2-R1441C cultures exhibited a decrease in lysosomal calcium release from TRPML1 channels, which may in turn lead to the increase in lysosomal calcium content we observe. Interestingly, it has previously been reported that the opening probability and ion conductance of the TRPML1 channel is dependent on lysosomal pH, with increased pH decreasing function (62). It is therefore plausible that the primary deficit underlying the LRRK2-R1441C phenotype we describe here is a defective lysosomal pH, with alterations in lysosomal calcium release being secondary to this. Lysosomal pH is implicated in lysosomal calcium loading (63) with alkaline pH decreasing the activity of H⁺ pumps speculated as being responsible (64). However, it has recently been demonstrated that the inhibition of vATPase H⁺ pumps does not prevent lysosomal calcium refilling (65). It is therefore possible that the physiological mechanisms behind lysosomal calcium loading are not as fully understood as previously thought.

The zinc/copper ionophore, clioquinol, was capable of rescuing the LRRK2-R1441C phenotypes described, increasing autolysosome maturation, lysosomal protein degradation and decreasing lysosomal pH. Furthermore, we demonstrated that, with clioquinol treatment, the expression of the $\alpha 1$ subunit of v-ATPase significantly increased from its reduced basal levels. Using the zinc chelator TPEN, we further showed that the therapeutic role of clioquinol was dependent on its ability to mobilize zinc into the lysosome. It is noticeable that with clioquinol treatment, LRRK2-R1441C cultures demonstrate significantly higher increase in zinc containing lysosomes to nTGs. Patients with PD have been reported to exhibit increased levels of both zinc and manganese in serum and cerebrospinal fluid (66,67). Whether this exaggerated increase in lysosomal zinc levels is indicative of increased intracellular basal levels in LRRK2-R1441C cells remains to be determined. Nonetheless, a role of metal ions in neurodegenerative disease is becoming more apparent (68,69).

In summary, our data highlight specific novel phenotypes caused by LRRK2 mutations and reveal further insight into normal physiological function of the WT protein. We demonstrate how two different mutations in different enzymatic cores of the same protein manifest in two very different phenotypes in the same cellular pathway, helping to ascribe a distinct function to the two enzymatic cores of LRRK2. We propose that the role of LRRK2 at the lysosome, specifically in regulating lysosomal pH and local calcium release by vATPase $\alpha 1$ binding and trafficking, is a crucial pathological mechanism linking autophagic deficits with Parkinson's. The demonstration that small molecules that directly target lysosome dysfunction, such as clioquinol, have potential therapeutic benefit for PD fits closely with the emerging consensus from genetics on this critical area of cell biology.

Materials and Methods

Generation of primary cortical neurons

Transgenic male rats were bred with a pair of Sprague Dawley female to produce litters. P1 rats were tail clipped and marked for genotyping. A minimum of three animals per genotype

were pooled for each experiment. Brains were extracted and meninges were removed, and cortical areas were dissected and shredded into 0.5 mm pieces. Tissue was incubated at 37°C in Neurobasal-A medium (Life Technologies) plus 0.01% trypsin and 0.5 µg/ml DNase for 20 min. Trypsin was inactivated with foetal bovine serum containing Neurobasal-A medium and samples centrifuged at 1000 rpm at 37°C for 5 min. This was then replaced with wash media and centrifuged at 1000 rpm at 37°C for 3 min. Wash media was removed and replaced with growth media (Neurobasal-A media, 1× Anti-Anti, 2 mM L-glutamine, 1× Anti-Anti, 1.75 µg Fungizone, 1× B27). Tissue was triturated, and cells were counted and diluted for plating. Cells were kept at 37°C, 5% CO₂, 95% relative humidity and 50% of medium was replaced every 2 days. All assays were completed at DIV 14.

Immunostaining

Cells were fixed in methanol previously cooled to -20°C and then washed with DPBS. Paraffin embedded sections, cut to 8 µm, were dewaxed and rehydrated through a series of alcohol. Cells/slides were blocked for 60 min at room temperature then incubated with primary over night at 4°C. Samples were then washed and incubated with secondary antibodies for 1 h at room temperature and were then washed and incubated in 1 µg/ml DAPI (Life Technologies). Coverslips were mounted onto Superfrost® plus (VWR) microscope slides using Fluorsave reagent (Millipore). Samples were imaged using an Invitrogen™ EVOS™ FL Auto cell imaging system at 60× magnification and a Nikon™ A1R™ confocal at 100× magnification. Unless stated, all immunostaining data was obtained from β-III tubulin/MAP2-positive cells.

Co-localization imaging and analysis

A minimum of 60 neurons were imaged per experimental condition across three technical replicates. For image analysis, images were quantified using Cell Profiler™. Neurons were identified manually using β-III tubulin stain. Puncta (LC3/LAMP1/p62/YPet/58-k) were converted to greyscale and enhanced, suppressing background and using the Otsu method (to threshold brightness) and size exclusion, puncta were identified. Puncta were then overlaid onto each other to identify those co-localizing (see [Supplementary Materials](#)). The same pipeline was used for lysosensor and FluoZin-3AM/LysoTracker Red DND-99 imaging.

Western blotting

Cells were lysed in RIPA with protease and phosphatase inhibitors. Samples were loaded onto 4–15% Criterion Tris-HCl polyacrylamide gels (BioRad). Electrophoresis was performed at 150 V for ~45 min, and proteins were transferred to a polyvinylidene membrane using a Trans-Blot Turbo Transfer System (BioRad). Membranes were blocked for 1 h at room temperature and incubated with primary antibody in blocking solution overnight at 4°C. Membranes were washed with TBS-T and incubated in horseradish peroxidase-conjugated secondary antibody (BioRad) in blocking solution for 1 h. Membranes were washed in TBS-T and developed using ECL solution (Millipore) and imaged on a Chemidoc Touch imaging system (Biorad) and quantified using ImageLab.

Lysosensor imaging and quantification of lysosome pH

Lysosomal pH was measured using the LysoSensor™ Green DND-189 (Life Technologies). Briefly, primary cortical cultures were labelled with 100 nM LysoSensor™ Green DND-189 in growth media for 1 h and either immediately imaged or incubated for 10 min in pH-calibrated solutions. Nuclei were stained with Hoechst 33258 for 10 min, and cells were imaged using an Invitrogen™ EVOS™ FL Auto cell imaging system at 20× magnification. pH values were then calculated using a standard curve generated from the pH calibrations. pH-calibration solutions were generated in Hanks Buffered Salt solution (GIBCO, Life Technologies) containing 20 mM MES (4-Morpholineethanesulfonic acid), 110 mM KCl and 20 mM NaCl, supplemented with 30 µM nigericin and 15 µM monensin, sterile filtered and titrated to pH values of 3, 4, 5, 6 and 7.

¹⁴C-valine pulse-chase protein degradation assay

¹⁴C-valine was added to each well of cells for 48 h at 37°C in a humidified incubator with 5% CO₂. Cells were then washed with fresh media and incubated for a further 24 h in the final wash. After 24 h, media was replaced with fresh media containing 1 mM ¹⁴C-valine. A total of 10 µM chloroquine was added to control wells to ensure radioactive counts measured were due to lysosomal protein degradation. Aliquots of media were collected from each well at various time points and proteins precipitated by adding to ice-cold 20% trichloroacetic acid. Samples were centrifuged at 17000g for 10 min to pellet the proteins, and the supernatant was transferred to a scintillation vial and scintillation fluid added. At the end of the time course the remaining media was removed and the cells lysed by addition of 0.1 M sodium hydroxide for 5 min at 37°C. The lysate was transferred to a scintillation vial and scintillation fluid added. Counts were measured using a scintillation counter and protein degradation by autophagy calculated as follows: % = 100 × (total counts for supernatant/total counts for supernatant and lysate). The % calculated for chloroquine treated samples were subtracted from those of untreated samples to ensure the final values were representative of lysosomal protein degradation.

Calcium imaging

Cortical cultures were incubated with 2.5 mM Fura2-AM (Molecular Devices) in calcium-free HBSS (ThermoFisher) supplemented with 20 mM HEPES and 0.02% pluronic F-127 (ThermoFisher) for 1 h and imaged on a FlexStation 3 Multi-Mode Microplate Reader (Molecular Devices). Light excitation at 340 nm and 380 nm and measurement of detection at 510 nm allowed the ratio of unbound:bound calcium signal to be calculated (F340/F380). After establishing a baseline signal for 30 s, calcium compounds were injected into wells and the ratio measured for 60/120 s. $\Delta (F_1 - F_0)$ was calculated to assess calcium store content.

Co-immunoprecipitation

Dynabeads™ Protein G (Invitrogen) were washed in PBS +/- using a magnetic rack (BioRad) and incubated with 40 µg of antibody/sample overnight at 4°C while rotating. Beads were washed in PBS +/-, and beads were then incubated with cell lysates (150 µg) for 3 days at 4°C while rotating. Flow through was removed for analysis and beads washed in PBS +/- and boiled at 65°C in 3× Laemmli sample Buffer and assessed by SDS-PAGE.

Zinc imaging

Cortical cultures were incubated with 5 μM FluoZin-3AM (Life Technologies) and 100 nM LysoTracker Red DND-99 (Life Technologies) for 1 h in neuronal growth medium supplemented with 0.02% pluronic acid F127 (Life Technologies). Cells were washed to remove unbound dye and incubated for 30 min to allow for the de-esterification of the dye. Nuclei were stained with Hoechst 33258 for 10 min and imaged on an Invitrogen™ EVOS™ FL Auto cell imaging system at 20 \times magnification.

Statistics and data analysis

Data and statistical analyses were performed using SPSS. Data were analyzed by either one-way or two-way analysis of variance (ANOVA) or by t-test. In instances when data did not fit parametric assumptions, Kruskal-Wallis non-parametric ANOVA was used. Post hoc tests following ANOVAs were conducted using Tukey HSD or Bonferroni correction. Two-tailed levels of significance were used, and $P < 0.05$ was considered statistically significant.

Supplementary Material

Supplementary Material is available at HMG online.

Acknowledgements

We acknowledge Milena Cioroch for expert technical assistance in breeding and maintenance of transgenic rat colonies.

Conflict of Interest statement. None declared.

Funding

Monument Trust Discovery Award from Parkinson's UK (grant J-1403 to R.W.-M.). R.W. holds the Joan Pitts-Tucker/Moritz studentship.

Authors contributions

R.W.-M. devised the study. R.W. performed analyses and experimental work and statistics. R.W.-M. & N.C.-R. supervised the study. All authors wrote, read and approved the final manuscript.

References

- von, S., Bornschein, B., Wick, R., Bötzel, K., Sampaio, C., Poewe, W., Oertel, W., Siebert, U., Berger, K. and Dodel, R. (2005) Prevalence and incidence of Parkinson's disease in Europe. *Eur. Neuropsychopharmacol.*, **15**, 473–490.
- Singleton, A.B., Farrer, M.J. and Bonifati, V. (2013) The genetics of Parkinson's disease: progress and therapeutic implications. *Mov. Disord.*, **28**, 14–23.
- Nalls, M.A., Pankratz, N., Lill, C.M., Do, C.B., Hernandez, D.G., Saad, M., DeStefano, A.L., Kara, E., Bras, J., Sharma, M. et al. (2014) Large-scale meta-analysis of genome-wide association data identifies six new risk loci for Parkinson's disease. *Nat. Genet.*, **46**, 989–993.
- West, A.B., Moore, D.J., Choi, C., Andrabi, S.A., Li, X., Dikeman, D., Biskup, S., Zhang, Z., Lim, K.L., Dawson, V.L. and Dawson, T.M. (2007) Parkinson's disease-associated mutations in LRRK2 link enhanced GTP-binding and kinase activities to neuronal toxicity. *Hum. Mol. Genet.*, **16**, 223–232.
- Greggio, E., Jain, S., Kingsbury, A., Bandopadhyay, R., Lewis, P., Kaganovich, A., Van Der, M.P., Beilina, A., Blackinton, J., Thomas, K.J. et al. (2006) Kinase activity is required for the toxic effects of mutant LRRK2/dardarin. *Neurobiol. Dis.*, **23**, 329–341.
- Heo, H., Park, J., Kim, C., Han, B., Kim, K. and Seol, W. (2010) LRRK2 enhances oxidative stress-induced neurotoxicity via its kinase activity. *Exp. Cell Res.*, **316**, 649–656.
- Lewis, P.A., Greggio, E., Beilina, A., Jain, S., Baker, A. and Cookson, M. (2007) The R1441C mutation of LRRK2 disrupts GTP hydrolysis. *Biochem. Biophys. Res. Commun.*, **357**, 668–671.
- Xiong, Y., Yuan, C., Chen, R., Dawson, T.M. and Dawson, V.L. (2012) ArfGAP1 is a GTPase activating protein for LRRK2: reciprocal regulation of ArfGAP1 by LRRK2. *J. Neurosci.*, **32**, 3877–3886.
- Sloan, M., Alegre-Abarrategui, J., Potgieter, D., Kaufmann, A., Exley, R., Deltheil, T., Threlfell, S., Connor-Robson, N., Brimblecombe, K., Wallings, R. et al. (2016) LRRK2 BAC transgenic rats develop progressive, L-DOPA-responsive motor impairment, and deficits in dopamine circuit function. *Hum. Mol. Genet.*, **25**, 951–963.
- Ramonet, D., Daher, J., Lin, B., Stafa, K., Kim, J., Banerjee, R., Westerlund, M., Pletnikova, O., Glauser, L., Yang, L. et al. (2011) Dopaminergic neuronal loss, reduced neurite complexity and autophagic abnormalities in transgenic mice expressing G2019S mutant LRRK2. *PLoS One*, **6**, 1–15, e18568.
- Li, Y., Liu, W., Oo, T., Wang, L., Tang, Y., Jackson-Lewis, V., Zhou, C., Gekhman, K., Bogdanov, M., Przedborski, S. et al. (2009) Mutant LRRK2 (R1441G) BAC transgenic mice recapitulate cardinal features of Parkinson's disease. *Nat. Neurosci.*, **12**, 826–828.
- Tong, Y., Yamaguchi, H., Giaime, E., Boyle, S., Kopan, R., Kelleher, R. and Shen, J. (2010) Loss of leucine-rich repeat kinase 2 causes impairment of protein degradation pathways, accumulation of alpha-synuclein, and apoptotic cell death in aged mice. *Proc. Natl. Acad. Sci. U. S. A.*, **107**, 9879–9884.
- Klionsky, D.J., Elazar, Z., Seglen, P.O. and Rubinsztein, D.C. (2008) Does bafilomycin A1 block the fusion of autophagosomes with lysosomes? *Autophagy*, **4**, 849–950.
- Pryor, P.R., Mullock, B.M., Bright, N.A., Gray, S.R. and Luzio, J.P. (2000) The role of intraorganellar Ca(2+) in late endosome-lysosome heterotypic fusion and in the reformation of lysosomes from hybrid organelles. *J. Cell Biol.*, **149**, 1053–1062.
- Korolchuk, V.I., Saiki, S., Lichtenberg, M., Siddiqi, F., Roberts, E., Imarisio, S., Jahreiss, L., Sarkar, S., Futter, M., Menzies, M. et al. (2011) Lysosomal positioning coordinates cellular nutrient responses. *Nat. Cell Biol.*, **13**, 453–460.
- Cuervo, A.M. and Dice, J.F. (2000) Age-related decline in chaperone-mediated autophagy. *J. Biol. Chem.*, **275**, 31505–31513.
- Miura, E., Hasegawa, T., Konno, M., Suzuki, M., Sugeno, N., Fujikaken, N., Geisler, S., Tabuchi, M., Oshima, R., Kikuchi, A. et al. (2014) VPS35 dysfunction impairs lysosomal degradation of α -synuclein and exacerbates neurotoxicity in a drosophila model of Parkinson's disease. *Neurobiol. Dis.*, **71**, 1–13.
- Zimprich, A., Benet-Pages, A., Struhal, W., Graf, E., Sebastian, M., Haubenberger, D., Spielberger, S., Lichtner, P., Klopp, N., Wolf, E. et al. (2011) A mutation in VPS35, encoding a subunit of the retromer complex, causes late-onset Parkinson disease. *Am. J. Hum. Genet.*, **89**, 168–175.

19. Chang, D., Nalls, M.A., Hallgrimsdottir, I.B., Hunkapiller, J., van der, M., Cai, F., International Parkinson's Disease Genomics Consortium and Me Research Team, Kerchner, G., Ayalon, A. et al. (2017) A meta-analysis of genome-wide association studies identifies 17 new Parkinson's disease risk loci. *Nat. Genet.*, **49**, 1511–1516.
20. Lees, A.J. and Singleton, A.B. (2007) Clinical heterogeneity of ATP13A2 linked disease (Kufor-Rakeb) justifies a PARK designation. *Neurology*, **68**, 1553–1554.
21. S, E., Nalls, M., Aasly, J., Aharon-Peretz, J., Annesi, G., Barbosa, E., Bar-Shira, A., Berg, D., Bras, J. et al. (2009) Multicenter analysis of glucocerebrosidase mutations in Parkinson's disease. *N. Engl. J. Med.*, **361**, 1651–1661.
22. Do, C.B., Tung, J., Dorfman, E., Kiefer, A., Drabant, E., Francke, U., Mountain, J., Goldman, S., Tanner, C., Langston, J. et al. (2011) Web-based genome-wide association study identifies two novel loci and a substantial genetic component for Parkinson's disease. *PLoS Genetics*, **7**, 1–14, e1002141.
23. Alegre-Abarrategui, J., Christian, H., Lufino, M., Mutihac, R., Venda, L., Ansoorge, O. and Wade-Martins, R. (2009) LRRK2 regulates autophagic activity and localizes to specific membrane microdomains in a novel human genomic reporter cellular model. *Hum. Mol. Genet.*, **18**, 4022–4034.
24. Alegre-Abarrategui, J. and Wade-Martins, R. (2009) Parkinson's disease, LRRK2 and the endocytic-autophagic pathway. *Autophagy*, **5**, 1208–1210.
25. Manzoni, C., Mamais, A., Roosen, D., Dihanich, S., Soutar, M., Plun-Favreau, H., Bandopadhyay, R., Hardy, J., Tooze, S., Cookson, M. et al. (2016) mTOR independent regulation of macroautophagy by leucine rich repeat kinase 2 via Beclin-1. *Sci. Rep.*, **6**, 1–10, 35106.
26. Gomez-Suaga, P., Churchill, G.C., Patel, S. and Hilfiker, S. (2012) A link between LRRK2, autophagy and NAADP-mediated endolysosomal calcium signalling. *Biochem Soc. Trans.*, **40**, 1140–1146.
27. Tong, Y., Giaime, E., Yamaguchi, H., Ichimura, T., Liu, Y., Si, H., Cai, H., Bonventre, J. and Shen, J. (2012) Loss of leucine-rich repeat kinase 2 causes age-dependent bi-phasic alterations of the autophagy pathway. *Mol. Neurodegener.*, **7**, 1–16.
28. Sergin, I., Evans, T., Zhang, X., Bhattacharya, S., Stokes, C., Song, E., Ali, S., Dehestani, B., Holloway, K., Micevych, P. et al. (2017) Exploiting macrophage autophagy-lysosomal biogenesis as a therapy for atherosclerosis. *Nat. Commun.*, **8**, 1–20, doi:10.1038/ncomms15750.
29. Gronostajski, R.M. and Pardee, A.B. (1984) Protein degradation in 3T3 cells and tumorigenic transformed 3T3 cells. *J. Cell Physiol.*, **119**, 127–129.
30. Manzoni, C., Mamais, A., Dihanich, S., McGoldrick, P., Devine, M., Zerle, J., Kara, E., Taanman, J., Healy, D., Marti-Masso, J. et al. (2013) Pathogenic Parkinson's disease mutations across the functional domains of LRRK2 alter the autophagic/lysosomal response to starvation. *Biochem. Biophys. Res. Commun.*, **441**, 862–866.
31. Sandor, C., Roberts, P., Lang, C., Heger, A., Booth, H., Vowles, J., Witty, L., Bowden, R., Hu, M., Cowle, S. et al. (2017) Transcriptomic profiling of purified patient-derived dopamine neurons identifies convergent perturbations and therapeutics for Parkinson's disease. *Hum. Mol. Genet.*, **26**, 552–566.
32. Seo, B.R., Lee, S.J., Cho, K.S., Yoon, Y.H. and Koh, J.Y. (2015) The zinc ionophore clioquinol reverses autophagy arrest in chloroquine-treated ARPE-19 cells and in APP/mutant presenilin-1-transfected Chinese hamster ovary cells. *Neurobiol. Aging.*, **36**, 3228–3238.
33. Sanchez-Danes, A., Richaud-Patin, Y., Carballo-Carbajal, I., Jimenez-Delgado, S., Caig, C., Mora, S., Di Guglielmo, C., Ezquerro, M., Patel, B., Giral, A. et al. (2012) Disease-specific phenotypes in dopamine neurons from human iPSC-based models of genetic and sporadic Parkinson's disease. *EMBO Mol. Med.*, **4**, 380–395.
34. Su, Y.C. and Qi, X. (2013) Inhibition of excessive mitochondrial fission reduced aberrant autophagy and neuronal damage caused by LRRK2 G2019S mutation. *Hum. Mol. Genet.*, **22**, 4545–4561.
35. Kihara, A., Kabeya, Y., Ohsumi, Y. and Yoshimori, T. (2001) Beclin-phosphatidylinositol 3-kinase complex functions at the trans-Golgi network. *EMBO Rep.*, **2**, 330–335.
36. Steger, M., Tonelli, F., Ito, G., Davies, P., Trost, M., Vetter, M., Wachter, S., Lorentzen, E., Duddy, G., Wilson, S. et al. (2016) Phosphoproteomics reveals that Parkinson's disease kinase LRRK2 regulates a subset of Rab GTPases. *Elife*, **5**, 1–28, e12813.
37. Stenmark, H. (2009) Rab GTPases as coordinators of vesicle traffic. *Nat. Rev. Mol. Cell Biol.*, **10**, 513–525.
38. Galea, G. and Simpson, J.C. (2015) High-content analysis of Rab protein function at the ER-Golgi interface. *Bioarchitecture*, **5**, 44–53.
39. Surmeier, D.J., Obeso, J.A. and Halliday, G.M. (2017) Selective neuronal vulnerability in Parkinson disease. *Nat. Rev.*, **18**, 101–113.
40. Giesert, F., Hofmann, A., Burger, A., Zerle, J., Kloos, K., Hafen, U., Ernst, L., Zhang, J., Vogt-Weisenhorn, D. and Wurst, W. (2013) Expression analysis of Lrrk1, Lrrk2 and Lrrk2 splice variants in mice. *PLoS One*, **8**, 1–15, e63778.
41. Thévenet, J., Pescini, G., Gobert, R., Hooft van Huijsduijnen, R., Wiessner, C. and Sagot, Y.J. (2011) Regulation of LRRK2 expression points to a functional role in human monocyte maturation. *PLoS One*, **6**, e21519.
42. Coffey, E.E., Beckel, J.A., Laties, A.M. and Mitchell, C.H. (2014) Lysosomal alkalization and dysfunction in human fibroblasts with the Alzheimer's disease-linked presenilin 1 A246E mutation can be reversed with cAMP. *Neuroscience*, **263**, 111–124.
43. Lee, J., Yu, W., Kumar, A., Lee, S., Mohan, P., Peterhoff, C., Wolfe, D., Martinez-Vicente, M., Massey, A., Sovak, G. et al. (2010) Lysosomal proteolysis and autophagy require Presenilin 1 and are disrupted by Alzheimer-related PS1 mutations. *Cell*, **141**, 1146–1158.
44. L, S., Sato, Y. and Nixon, R.A. (2011) Lysosomal proteolysis inhibition selectively disrupts axonal transport of degradative organelles and causes an Alzheimer's-like axonal dystrophy. *J. Neurosci.*, **31**, 7817–7830.
45. Yang, J., Wu, L., Tashino, S., Onodera, S. and Ikejima, T. (2008) Reactive oxygen species and nitric oxide regulate mitochondria-dependent apoptosis and autophagy in evodiamine-treated human cervix carcinoma HeLa cells. *Free Radic. Res.*, **42**, 492–504.
46. Guicciardi, M.E., Marcel, L. and Gregory, G. (2004) Lysosomes in cell death. *Oncogene*, **23**, 2881–2890.
47. Lee, J., Kumar, A., Sato, Y., Mohan, P., Kompella, U. and Lloyd-Evans, E. (2015) Presenilin 1 maintains lysosomal Ca²⁺ homeostasis by regulating vATPase-mediated lysosome acidification. *Cell Rep.*, **12**, 1430–1444.
48. Cotter, K., Stransky, L., McGuire, C. and Forgacs, M. (2015) Recent insights into the structure, regulation and function of the V-ATPases. *Trends Biochem. Sci.*, **40**, 611–622.
49. Finnigan, G.C., Cronan, G., Park, H., Srinivasan, S., Quiocho, F. and Stevens, T. (2012) Sorting of the yeast vacuolar-type,

- proton-translocating ATPase enzyme complex (V-ATPase): identification of a necessary and sufficient golgi/endosomal retention signal in *stv1p*. *J. Biol. Chem.*, **287**, 19487–19500.
50. Namkoong, S., Lee, K., Lee, J., Park, R., Lee, E., Jang, I. and Park, J. (2015) The integral membrane protein ITM2A, a transcriptional target of PKA-CREB, regulates autophagic flux via interaction with the vacuolar ATPase. *Autophagy*, **11**, 756–768.
 51. Bagh, M.B., Peng, S., Chandra, G., Zhang, Z., Singh, S., Pattabiraman, N., Liu, A. and Mukherjee, A. (2017) Misrouting of v-ATPase subunit VOa1 dysregulates lysosomal acidification in a neurodegenerative lysosomal storage disease model. *Nat. Commun.*, **8**, 1–16, 14612.
 52. Bijlmakers, M.J. and Marsh, M. (2003) The on-off story of protein palmitoylation. *Trends Cell Biol.*, **13**, 32–42.
 53. Covy, J.P. and Giasson, B.I. (2009) Identification of compounds that inhibit the kinase activity of leucine-rich repeat kinase 2. *Biochem. Biophys. Res. Commun.*, **378**, 473–477.
 54. Luzon-Toro, B., De La, E., Delgado, A., Perez-Tur, J. and Hilficker, S. (2007) Mechanistic insight into the dominant mode of the Parkinson's disease-associated G2019S LRRK2 mutation. *Hum. Mol. Genet.*, **16**, 2031–2039.
 55. West, A.B., Morre, D., Biskup, S., Bugayenko, A., Smith, W., Ross, C., Dawson, V. and Dawson, T. (2005) Parkinson's disease-associated mutations in leucine-rich repeat kinase 2 augment kinase activity. *Proc. Natl. Acad. Sci. U. S. A.*, **102**, 16842–16847.
 56. Anand, V.S. and Braithwaite, S. (2009) LRRK2 in Parkinson's disease: biochemical functions. *FEBS J.*, **276**, 6428–6435.
 57. Biosa, A., Trancikova, A., Civiero, L., Glauser, L., Bubacco, L., Greggio, E. and Moore, E. (2013) GTPase activity regulates kinase activity and cellular phenotypes of Parkinson's disease-associated LRRK2. *Hum. Mol. Genet.*, **22**, 1140–1156.
 58. Li, X., Tan, Y., Poulouse, S., Olanow, C., Huang, X. and Yue, Z. (2007) Leucine-rich repeat kinase 2 (LRRK2)/ PARK8 possesses GTPase activity that is altered in familial Parkinson's disease R1441C/G mutants. *J. Neurochem.*, **103**, 238–247.
 59. Daniëls, V., Vancaenenbroeck, R., Law, B., Greggio, E., Lobbstaël, E., Gao, F., De Maeyer, M., Cookson, M., Harvey, K., Baekelandt, V. et al. (2011) Insight into the mode of action of the Lrrk2 Y1699C pathogenic mutant. *J. Neurochem.*, **116**, 304–315.
 60. Liao, J., Wu, C., Burlak, C., Zhang, S., Sahm, H., Wang, M., Zhang, Z., Vogel, K., Federici, M., Riddle, S. et al. (2014) Parkinson disease-associated mutation R1441H in LRRK2 prolongs the 'active state' of its GTPase domain. *Proc. Natl. Acad. Sci. U. S. A.*, **111**, 4055–4060.
 61. Xiong, Y., Coombes, C., Kilaru, A., Li, X., Gitler, A., Bowers, W., Dawson, V., Dawson, T. and Moore, D. (2010) GTPase activity plays a key role in the pathobiology of LRRK2. *PLoS Genet.*, **6**, 1–18, e1000902.
 62. Li, M., Zhang, W., Benven, N., Zhou, X., Su, D., Li, H., Wang, S., Michailidis, L., Tong, L., Li, X. et al. (2017) Structural basis of dual Ca²⁺/pH regulation of the endolysosomal TRPML1 channel. *Nat. Struct. Mol. Biol.*, **24**, 205–213.
 63. Christensen, K.A., Myers, J.T. and Swanson, J.A. (2002) pH-dependent regulation of lysosomal calcium in macrophages. *J. Cell Sci.*, **115**, 599–607.
 64. Churchill, G., Okada, Y., Thomas, J., Genazzani, A., Patel, S. and Galione, A. (2002) NAADP mobilizes Ca²⁺ from reserve granules, lysosome-related organelles, in sea urchin eggs. *Cell*, **111**, 703–708.
 65. Garrity, A.G., Wang, W., Collier, C., Levey, S., Gao, Q. and Xu, H. (2016) The endoplasmic reticulum, not the pH gradient, drives calcium refilling of lysosomes. *Elife*, **5**, 1–6, e15887.
 66. Fukushima, T., Tan, X. and Kanda, H. (2011) Serum vitamins and heavy metals in blood and urine, and the correlations among them in Parkinson's disease patients in China. *Neuroepidemiology*, **36**, 240–244.
 67. Hozumi, I., Hasegawa, T., Honda, A., Ozawa, K., Hayashi, Y., Hashimoto, M., Yamada, M., Koumura, A., Sakurai, T., Kimura, A. et al. (2011) Patterns of levels of biological metals in CSF differ among neurodegenerative diseases. *J. Neurol. Sci.*, **303**, 95–99.
 68. Sastre, M., Ritchie, C.W. and Nabil, H. (2015) Metal ions in Alzheimer's disease brain. *JSM Alzheimer's Dis. Related Dementia*, **2**, 1014.
 69. Ward, R.J., Dexter, D.T. and Crichton, R.R. (2015) Neurodegenerative diseases and therapeutic strategies using iron chelators. *J. Trace Elem. Med. Biol.*, **31**, 267–273.